Third United Nations International Conference on the Peaceful Uses of Atomic Energy

A/CONF.28/P/377
USSR
May 1964
Original: RUSSIAN

Confidential until official release during Conference

NEW RESULTS OF SHIELDING RESEARCH

O.I.Leypunsky, S.G.Tsypin, A.A.Abagyan, V.N.Avaev, S.P.Belov, E.B.Breshenkova, G.A.Vasilyev, A.P.Veselkin, V.K.Daruga, S.F.Degtyarev, V.A.Dulin, U.A.Egorov, U.A.Kazansky, L.R.Kimel, V.A.Klimanov, V.I.Kukhtevitch, E.S.Matusevich, V.P.Mashkovich, M.E.Netecha, A.V.Nikitin, V.V.Orlov, U.V.Orlov, U.V.Pankratyev, A.M.Panchenko, V.I.Popov, V.K.Saharov, B.I.Sinitsin, L.A.Trikov, B.P.Shemetenko

The results of new experimental and theoretical researches on different items of shielding are given in the present paper.

Section I presents data on the radiation field from the point monodirectional source which permits to receive data on the radiation field from sources of different shapes.

Section II contains detailed information on the angular energy and space distribution of a neutron flux and of gamma rays in the medium as well as on their boundaries of the production, the yield and the processes of suppression of capture gamma radiation on the optimization of shielding physical characteristics, on the spectral angular characteristics of radiation scattered in air.

Section III is dedicated to the experimental and theoretical determination of the dose build-up factor of the neutron radiation for various shielding media which presents some practical interest.

Section I

RADIATION FIELD FROM MONODIRECTIONAL SOURCES

A great configuration variety of radiactive sources encountered in all fields of atomic power application presents a problem in the radiation field definition in the shielding media surrounding the radiactive matter.

It stipulates a search for such simple sources, basing on the known radiation field of which, one may draw up the radiation field of any compound source configurations. The point monodirectional and monoenergetic source (narrow fine beam) which is the most elementary source gives wide latitude in the use.

The field of the point monodirectional source can be deduced by solution of the kinetic transport equation, by Monte Carlo or experimental methods.

A number of papers are dedicated to these studies [1–23]. The solution of the kinetic equation presents great difficulties and has not been conducted heretofore [7, 16, 21, 22]. The

calculations of the radiation field from a narrow beam with the initial energy of gamma-quanta of 0.66 Mev distributed in iron at distances up to 7 mean free paths and in air at distances less than a mean free path of the gamma-quanta and neutrons of different energies from a narrow beam have been calculated by the Monte Carlo methods. A great number of variables presents certain difficulties for the application of the Monte Carlo method. A deficiency in the theoretical data on the narrow beam radiation field induced experimental research.

§1. NARROW BEAM OF GAMMA-QUANTA RADIATION FIELD MEASUREMENT

A narrow beam was produced by the strong collimation of the radiation of the point isotropic sources Cs^{137}, Co^{60}, Na^{24}. The calculations were carried out in infinite geometry. A scintillation counter with an organic crystal and a small-size halogen counter with special filters, smoothing away the dependence of the reading of the detector from gamma-quantum energy [23], were used so that the readings of the detectors in pulses per minute were proportional to the scattering energy flux of Mev/cm^2 min materials, gamma-quantum energies and maximum distances are listed in Table 1 on which the functions of a narrow beam distribution have been studied. As an example Fig.1 gives the space distribution of the scattered energy. $\Phi_0(\vec{r}, \vec{r_0}, E_0, \vec{\Omega}_0$ in points $\vec{r}_0$ from a narrow beam with the initial energy of gamma-quantum $E_0 = 2.76$ Mev, emitted from the point $\vec{r}_0$ in the direction $\vec{\Omega}_0$ in Al. It should be noted that $\Phi_0(\vec{r}, \vec{r}_0, E_0, \vec{\Omega}_0) = \Phi_0(z, \rho)$ as it is assumed that $\vec{r}_0 = 0$, the beam is directed along the axis z, and z, ρ – are cylindrical coordinates; the distribution on φ is isotropic. The shape of the curve for the distribution functions $\Phi_0(z, \rho)$ given in Fig.1 is typical for other materials and energies. The functions $\Phi_0(z, \rho)$ are shown in Figure 2 for a number of materials from a narrow beam with the initial energy of 1.25 Mev for $\mu_0 z = 2$. Figure 3 shows the space energy distribution of gamma-quanta in water from a narrow beam with the initial quantum energy of 0.66 Mev $G_0(z, \rho, E)$ in the cylindrical system of coordinates.

The scattered radiation distribution in water from a narrow beam in the plane normal to the direction of the beam $\Phi_0(z, \rho)$ for the points standing from the source more than one mean free path may be expressed by:

$$\Phi_0(z, \rho) = E_0 e^{-\mu_0 z} \mu_0^2 \mu_0 z \Phi(\alpha \mu_0 \rho) \text{ Mev/cm}^2\text{sec} \qquad (1)$$

where E_0 – Mev/sec is the source strength; μ_0 the linear attenuation coefficient; $\Phi(\alpha\mu_0\rho)$ is the King function,

$$\alpha = \sqrt{\frac{2\pi \mu_0 z}{3(B-1)}}$$

B is the energy build-up factor of the plane monodirectional source. For the materials with the atomic numbers more than that of water, in expression (1) instead of $\Phi(\alpha \mu_0 \rho)$ should be used. $- E_i(-\alpha \mu_0 \rho)$

§2. MEASUREMENTS OF NEUTRON FIELD FROM DISK MONODIRECTIONAL SOURCE

The disk monodirectional source was used for the experimental studies due to its axial symmetry. The measurements of the distribution functions were carried out on the B-2 facility [12, 19] of the reactor BP-5, which was the disk monodirectional source with the diameter of 2a = 30 cm (see §1, section 2). The measurements were conducted in water, in Fe, and in C. As an example Figures 4, 5, 6 show some distribution functions of the pointed neutron fission source in water, measured by the P^{31} (n, p) reaction in Fe, Al^{27} (n, d) reaction and S^{32} (n,p) reaction in C. For comparison Fig.5 also gives the calculated data [16]. Fig. 7 gives the functions $\Phi^{disk}(z, \rho, a)$ for one thickness z = 30 cm, for a number of materials and for B-2 source, measured by S^{32} (n, p) reaction.

It is not difficult to show that for the space distribution functions one may make some transformations from the disk monodirectional source to the plane monodirectional source according to the following formula:

$$\Phi^{pl,\ monod.}(z) = C \int_0^{2\pi} d\varphi \int_0^{\infty} \Phi^{disk}(z, \rho, a)\rho d\rho \qquad (2)$$

Knowing the space distribution function from the disk monodirectional source $\Phi^{disk}(z, \rho, a)$ with the corresponding simplifying assumptions one may perform a retransformation to the narrow beam [13, 19].

Section II

DISTRIBUTIONS AND RADIATION PRODUCTION IN VARIOUS SHIELDING MEDIA

§1. FACILITIES FOR SHIELDING RESEARCH

The facility B-2 [12] was established on the fast neutron reactor BP-5 [24] for investigation of neutron passage through various shield materials and assemblies (see Fig.8). The essential difference of B-2 from the facilities known in the literature is the use of the disk monodirectional source which permits to obtain more detailed information concerning the shield under the investigation (see Fig.9). The reactor "PIT" is a zero-power uranium –water reactor for the investigation of the production, yield and the processes of suppression of capture gamma radiation in the shielding (see Fig.10). The special top-shield made from B_4C and B_i permits to acquire a good ratio between the emerging neutrons and the gamma-ray fluxes.

§2. NEUTRON PASSAGE

The fast neutron passage of the reactor BP-5 with the energy of E > 2–3 Mev in LiH and in C infinite geometry was studied. The measurement results given in Fig. 11 are compared with the calculations [9, 25]. The satisfactory agreement between experiments and calculations testifies the accuracy of calculated method and the proper chosen cross-sections. In media which contain no hydrogen the neutron flux distribution with the energy of E > 2–3 Mev for the shielding thicknesses R from 2 to 15–20 mean free paths is approximated by the following expression: $\Phi(R) \sim \exp(-qR)$, where the following values may be used as q: the removal cross-sections Σ rem, if one considers the neutron group with the energy above 3 Mev [26],

the cross sections obtained by reciprocal relaxation lengths $\Sigma_{1/\lambda}$ for the neutron group with the energy above 3Mev [26]; the asymptotic cross-sections, obtained from the solution of the one-velocity kinetic equation in the transport approximation [26] by using the group constant system [27], [28] for the groups with the energy of $1.4 - \infty$, $2.5 - \infty$ Mev.

Table II presents these parameters taken from the numerous literature sources or obtained by the authors of the present report who studied experimentally the neutron passage in the infinite extended shielding media of C, Na, Fe and also in ferrum-carbon and ferrum oxigen mixtures.

The angular energy distribution of fast neutrons was experimentally investigated by the method presented in [29, 30]. The reaction D(D, n) He^3 serving as a neutron source (3.4 Mev energy). As an example Fig.12 shows the angular distributions of neutron energy groups for H_2O, C, Fe and Pb. The angular dependence of the scattered neutron groups in the solid angle $d\Omega$ in the range of 3.1 to 3.4 Mev can be presented as $\exp(\theta/\theta_0)$ where θ for H_2O, C and Al is about 20°, and for the media with $A > 30 \sim 35^\circ$. The angular distribution of the fast-neutron dose with the energy over 0.4Mev for media with $A > 30$ may be presented as the same function with the parameter $\frac{2}{3}\pi \leqslant \theta_0 \leqslant \pi$ for H_2O and angles $\theta > 10^\circ$, $\theta_0 \sim 45^\circ$. Angular distribution representation as a monoparameter function is accurate within 10%.

§3. CAPTURE GAMMA-RADIATION AND SHIELD OPTIMIZATION

It is advisable to introduce experimental parameters characterizing the capture gamma-ray output from various shields. One of such parameters is the secondary gamma-radiation coefficient β, equal to the ratio of the total gamma-quantum number emerging from the shield to the total number of the neutrons having left the shield [31]. Starting from a definite thickness of the shielding β was proved to be constant and was defined only by the media properties. Fig.13 shows β coefficients measured on "РИЗ" reactor for Fe, Ni, homogeneous mixture of Ni with B. Boron-containing additions injected into the shield can decrease the capture gamma-ray output. Boron -injection was found to decrease gamma-ray output effectively only at its small quantities (up to 2–3% weight). Fig.14 gives the characteristic dependence of the gamma-ray output from Fe and Ni on the boron weight concentration.

Various shield characteristics may be given as:

$$J_k = \int \Phi(\vec{r}, \vec{\Omega}, E) P_k(\vec{r}, \vec{\Omega}, E)\, d\vec{r}\, d\vec{\Omega}\, dE + \varphi[\rho_i(r)]$$

Shield weight is functional: $P_k = \int \sum_i \rho_i(\vec{r})\, dv$

where: Φ – neutron flux, P_k – characterizes the process, stimulated by neutrons (capture gamma-radiation, heat generation and so on). φ – is defined by the external gamma-radiation sources. ρ_i – is material density.

Shield optimization task can be put as follows. Minimum J_0 value must be found on condition that J_1 ..... J_k ..... J_m values do not exceed same definite value. Shield material efficiency functions f_{ij}^k (k = 0.1 ....m) [32] characterizing variation of functionals J_k while introducing a single quantity of i material into j point can be calculated by utilizing adjoint

function method and perturbation theories. Let us introduce (m+1) – dimensional space the components of which are ΔJ_0, ΔJ_1 .....ΔJ_m and separate from it the direction of the minimizing value $J_0 - \vec{S}_0$. Shield material distribution $\rho_i(\vec{r})$ where $\vec{f}_{ij}$ vectors with f_{ij}^k components form a convex cone which does not contain a vector with minimizing direction S_0 is considered to be optimum.

Note that shield material efficiency functions may be obtained experimentally and on this basis optimization can be experimentally yielded. Hydrogen efficiency function $\rho_H = 0.111\ g/cm^3$ in Nickel $f_{Hj}(r)$ in relation to capture gamma-radiation was obtained on reactor "РИЗ" (Fig.15). The same function was calculated by the perturbation theory expressing [32]. Fig. 15 shows that the agreement is satisfactory. f_{Hj} dependence in maximum from hydrogen value was experimentally shown to be linear up to 0.11 gr/cm^3 hydrogen content.

§4. NEUTRON AND GAMMA-RAY SCATTERING IN AIR

In the area of R-distances negligible as against the free-path length $1/\Sigma_t(E_0)$ there take place compensation of the multiple scattered radiation accumulation and absorption. As a result of it space distribution of the flux or dose rate is proportional to 1/R (R – the distance source-detector). This relationship was experimentally proved by the authors and is following from calculation works [9,33–36]. The relationship 1/R essentially simplifies the description of the scattered radiation distribution from various sources in the air.

Having introduced the relative flux N_n defined by the ration of the scattered neutron flux in the air to the flux in vacuum in the same place, space distribution N_n from the point isotropic source can be given as $N_n(R, E_0) = (2.15 \pm 0.2) R [\Sigma_t(E_0) - \Sigma_a(E_0)] \alpha(E_0)$ where $\Sigma_a(E_0)$ is absorption cross-section, $\alpha(E_0) = 1$ for $E_0 < 6$ Mev and smoothly swifts to 0.8 at $E_0 = 14$Mev. By analogy we have $D_n(R, E_0) = B(E_0) \sqrt{\Sigma_t(E_0)} R$ for the relative dose rate D_n, where $B(E_0) = 0.195 \pm 0.02$ for $E_0 = 0.1$–6Mev and 0.145 ± 0.015 for E = 7–14 Mev. N_n and D_n values are dependent $N_n(R, E_0) = (1.1–1.2) D_n(R, E_0)$.

Experimental and calculation values show that within the accuracy ±20%, geometry of monodirectional source-isotropic detector is equivalent to an isotropic source monodirectional detector. In such a case their corresponding relating dose rate distributions P_n and Q_n can be given as:

$$P_n(R, E_0, \eta) = 2.2\sqrt{\Sigma_t} \cdot R_\eta^{\varkappa(E_0, \eta)} \quad \text{and} \quad Q_n(R, E_0, \Psi) = 2.2\sqrt{\Sigma_t} R \Psi^{\varkappa(E_0, \Psi)},$$

where η and Ψ are orientation angles of the monodirectional source and detector correspondingly $\varkappa(E_0)$ for $E_0 = 0.1 - 14$ Mev changes in the range from 1.1 to 1.4 for η and Ψ from 5 to 120°. Fig. 16 illustrates the relationship of P_n from η.

Fig.17 illustrates the comparison of two geometries: the point isotropic source – monodirectional detector (experiment) and the point monodirectional source – isotropic detector (calculation). Fig. 17 shows that neutron spectrum degradation from orientation angle is small and energy distributions are close for both geometries.

Space distribution of relative dose rate of scattered gamma-rays $0.5 \leq E_0 \leq 10$Mev from isotropic source without taking into account annihilation radiation has the following expression,

$$D_\gamma(E_0, R) = 4.3 \cdot 10^{-2} R \left[(7.7 - \frac{4.2}{1+\exp(-\frac{E_0 - 2.5}{0.1})}) E_0 + \frac{9}{1+\exp(-\frac{E_0 - 2.5}{0.1})}\right]^{-1} \pm 20\%$$

where $E_0 = 6$ Mev, and R in m.

Space distribution of relative dose rate of scattered gamma-rays in the air from a point monodirectional source has the expression:

$$P_\gamma(E_0, R, \eta) = \begin{cases} \frac{0.48}{E_0} R\eta^{-1.78} & 20^\circ < \eta < 90^\circ \\ \frac{1.12 \cdot 10^{-2}}{E_0} R\eta^{-0.95} & 90^\circ < \eta < 180^\circ \end{cases}$$

for energy E_0 from 0.4 to 1.5 Mev without taking into account anihilation radiation.

$$P_\gamma(E_0, R, \eta) = \frac{LC(\eta)(\pi - \eta)R}{T(E_0)\sin\eta}$$

for energy E_0 more than 2 Mev L is constant here, $C(\eta)$ is compton differential cross-section, $T(E_0)$ is gamma-ray dose rate with E_0 energy. $P_\gamma(\eta)$ changes as R distance increases, Fig. 18 illustrating it. Fig. 19 shows the reversibility of geometry for gamma-rays which takes place by analogy with neutrons. This Fig. gives the experimental values of energy distribution for $E_0 = 1.25$ Mev $\eta = \Psi = 60^\circ$ and $R = 16$ m from monodirectional source $P_\gamma(E)$ (isotropic detector) and from isotropic source $q_\gamma(E)$ (monodirectional detector).

Fig.20 shows how much the calculation in single approximation underestimates the "soft" part of the spectrum. The calculation distribution was "spoiled" by the energetic resolution of the spectrometer.

Section III

NEUTRON DOSE BUILD-UP FACTOR

Dose rate calculation method from neutrons of reactor spectrum is offered in this article. This method is based on the utilization of the removal cross-section method, kinetics equation solution multigroup method of neutron transfer and introduction of dose build-up factor notion of neutron radiation analogous in form to the corresponding notion for gamma-quantum.

Recently semiempirical removal cross-section method has developed and is widely used in calculations. It enables to define fast neutron attenuation with energy above 2–3 Mev with certain simplicity. Hence, for neutron radiation, dose build-up factor is convenient to be normalized on the fast neutron dose rate. In order to determine dose built-up factor in relation to fast neutron group kinetics equation solution multigroup method of neutron transfer in age-diffusion approximation exactly taking into account moderation in hydrogen. On the basis

of N. group neutron flux calculations and conversion factors of neutron flux into dose rate [39] dose rate space distributions were calculated for each energetic neutron group $D_j(r)$. Dose build-up factor was calculated by the expression:

$$B(r) = \sum_{j=1}^{N} (D)_j (r)/D_1 (r) \qquad (3)$$

Two groups of questions are investigated.

1. Energetic and space dose rate distribution from neutrons in homogeneous protective material media in infinite geometry. In this case the outer boundary of the investigated protective layer was supposed to be black.

2. Energetic and space dose rate distribution from neutrons in various combinations of protective materials, imitating by themselves the possible combinations of the last biological shielding layers. In this case geometry, generally speaking, is barrier, but distorted by the presence of man and the scattering from surrouding walls and structures. Hence it was decided to place 20 cms of polyethylene, nuclear-physical properties of which are close to that of the biological tissue to behind the last layer of the composition, and to make the multigroup fluxes equal to zero on the extrapolated boundary beyond the indicated material.

§1. NEUTRON SPECTRUM MEASUREMENT AND DOSE CALCULATION

The succession of dose rate calculation from neutrons of reactor spectrum is the following. By the removal cross-section method dose rate was calculated first from fast neutrons with utilization of dose attenuation curves in hydrogenous shield. Then the dose build-up factor was chosen according to the concrete composition of the biological shielding outer part.

Spectral distribution measurements of neutrons within 0.9 – 13 Mev for some homogenous shielding materials among them for serpentine, for mixture of polyethylene, iron and lead and for mixture of graphite and iron were made for averaging nuclear-physical constants in the range of 10 MeV > E_n > 0.7 MeV in addition to the known data [25, 40].

Constants for neutrons within 0.7 MeV ≥ E_n > 0.4 ev were averaged on asymptotic spectra of slowing down neutrons. In a number of materials it was necessary range to measure neutron spectrum in epithermal energy especially.

Energy distribution measurements of fast and intermediate neutrons were produced on water-moderated water-cooled research reactor. Fast neutron spectra in the range of 0.9 – 13 MeV were measured in the conditions of barrier geometry. For measurements single-crystal scintillation spectrometer was used with stilbene crystal and gamma-background discrimination.

There were measured spectra of fast neutrons having passed through different layer thickness of homogenous materials such as polyethylene [41], graphite, iron (St–3), lead [40] and through different layer thickness of mixtures of iron with polyethylene, lead with polyethylene, iron with graphite. As well fast-neutron spectrum deformation was investigated when passing through serpentinite (SiO_2 – 39%, MgO – 37%, H_2O – 11.5%, Fe_2O_3 – 8.5%).

Energy distribution of epithermal neutrons was investigated with the help of a number of radioactive resonance indicators by "comparison with 1/E" method. Measurements were car-

ried out in semi-infinite geometry conditions. Indicator-set enabled to define spectral-line shape in the range of 0.46 ev up to 6 kev. As an example energy distributions of fast neutrons in the mixture of polyethylene + iron are given in Fig. 21. Energy distribution of epithermal neutrons in iron and graphite with boron is given in Fig. 22.

§2. CALCULATION OF DOSE BUILD-UP FACTORS

Using formula 3 we calculated dose build-up factors in the following homogeneous materials: water, homogeneous water-iron shielding with 50% iron content by volume, polyethylene, polyethylene with 2.5% natural boron content by weight, serpentine concrete, graphite and boron mixture (8% boron by weight), titanium hydride titanium hydride with 2.5% boron content by weight, iron, iron with 0.8% boron by weight, lead and graphite.

Besides there was studied the contribution into the total dose from neutrons of various energetic groups in compositions of shieldings representing possible arrangement of the last layers of the real biological shielding.

In all compositions hydrogenous medium was chosen as the first layer, it being of such thickness so as the equilibrium spectrum was established in it, i.e., as in a real case, energy distribution of neutrons in the last layers was defined by the neutrons of the first group. The following media were considered as the first layers: water, serpentine concrete, water-iron mixture, polyethylene with boron and titanium hydride.

Lead of different thickness was taken as the second layer in all the considered compositions.

While designing biological shielding of nuclear power plants there are two ways to produce the desired total dose rate either to increase the thickness of their basic shielding material (the first layer) or to add a blocking material layer after lead which at small thickness would cut build-up factor to a minimum feasible value.

In this report two hydrogenous materials were studied as a blocking layer: polyethylene with boron and titanium hydride with 2.5% boron content by weight.

EXPERIMENTAL DETERMINATION OF DOSE BUILD-UP FACTORS CALCULATED AND EXPERIMENTAL DATA COMPARISON

Experimental measurements of dose build-up factors were carried out for polyethylene, serpentinite, titanium hydride with boron and a composition consisting of 50 cm polyethylene and 10 cm lead. The build-up factor was defined as a ratio of two values: total dose rate from all energy neutrons and dose rate due to neutrons with $E_n \geqslant 2$ Mev.

Total dose rate was defined with the isodose detector [42]. Fast-neutron dosimeter with a plexiglass tablet of $Z_nS(Ag)$ in the detecting element with $E > 2$ Mev was used for measuring dose rate of neutrons.

Table III represents experimental and calculated data according to build-up factors for given homogeneous materials and the composition.

As seen from the comparison of the calculated and experimental data the difference between the calculated dose build-up factors and measured ones does not exceed 20%.

The materials, gamma-quantum energies and maximum distances (in the mean free path lengths) with the help of the narrow ray distribution functions were investigated.

Table 1

Investigated materials	Energy γ-quantum E_0, Mev					
	0.66		1.25		2.76	
	$\mu_0 z$	$\mu_0 \rho$	$\mu_0 z$	$\mu_0 \rho$	$\mu_0 z$	$\mu_0 \rho$
Water	4	3	4	2	—	—
Aluminium	7	3	5	3	3	2
Concrete	6	3	4	2	—	—
Iron	7	4	5	3	4	3
Lead	6	4	5	3	3	3

The comparison of removal cross sections, cross sections produced by reciprocal relaxation lengths and asymptotic cross sections.

Table II

Element	σ_{rem}[37] barn	$\sigma 1/\lambda$ barn	σ_{as} barn	
			1.4 – ∞ Mev	2.5 – ∞ Mev
Lithium	1.01	1.07	1.03 [28]	
Beryllium	1.07	1.15 [9]	1.20 [28]	
Boron	0.97	1.12 [38]	1.12 [28]	
			1.00 [27]	
Carbon	0.81	0.75	0.95 [27]	
Oxygen	0.74		0.74 [27]	
Sodium	1.26	1.50	1.36 [27]	
Magnesium	1.29		1.35 [27]	
Aluminium	1.30		1.42 [27]	
Silicon	1.37		1.23 [28]	
Potassium	1.57		1.54 [28]	
			1.39 [27]	
Titanium	1.82		1.62 [27]	
Chromium	1.77		1.98 [27]	
Iron	1.98	1.81 [8]	1.87 [28]	
Nickel	1.89	1.90 [26]	1.84 [27]	
Copper	2.04		2.04 [28]	
Zirconium	2.36		2.43 [27]	
Niobium Columbium	2.37		2.30 [28]	
Molybdenum	2.38		2.85 [28]	
Barium	2.82		3.14 [28]	
Tungsten	3.36		3.94 [27]	
Lead	3.70		2.63 [27]	3.33 [27]
Bismuth	3.50		2.62 [27]	3.53 [27]

* The value $\sigma 1/\lambda$ for B was got from the measurements $\sigma 1/\lambda$ for B_4C [38] and $\sigma 1/\lambda = 0.75$ for carbon.

377

Calculated and experimental values of dose build-up factors for various materials and one composition.

Table III

Material	Polyethylene	Serpentinite	Titanium hydride with boron	50 cm polyethylene + 10 cm lead
Build-up factor experimental value	2.1	2.05	2.76	3.25
Build-up factor calculated value	1.9	2.45	2.4	3.35

377

LIST OF REFERENCES

1. *L.V.Spenser, F.Stinson*, Phys. Rev., 85, (1952), 662.
2. *W.P.Stinson*, Nucleonics, 12 (1954), 500.
3. Защита ядерных реакторов под ред. *Т.Рокселла*, изд. ИЛ. Т., 1958.
4. *M.I.Berger, L.F.Spenser*, Rad. Res., 10 (1959), 552.
5. *В.А.Дулин, Ю.А.Казанский, В.П.Машкович, Е.А.Панов, С.Г.Цыпин*, журнал "Атомная энергия", 9 (1960), 315.
6. *В. А.Дулин* и др., журнал "Атомная энергия", 9 (1960), 318.
7. Е.Б.Бреженкова, В.В.Орлов, журнал "Атомная энергия", 10 (1961), 175.
8. *В.П.Машкович, С.Г.Цыпин*, журнал "Атомная энергия", 11 (1961), 251.
9. Reactor Handbook, v.III Part B Shielding, *E.P.Blizard*, Editor, ORNL, New York, London, 1962.
10. *В.П.Кухтевич, Б.П.Шеметенко*, журнал "Атомная энергия, 12 (1962), 204.
11. *Л.Р.Кимель, О.П.Лейпунский*, журнал "Атомная энергия", 12 (1962), 236.
12. *С.Г.Цыпин*, журнал "Атомная энергия", 12 (1962), 300.
13. *В.П.Машкович*, статья в сб. "Вопросы дозиметрии и защиты от излучений", под ред. *В.И.Иванова*, вып. 1, Госатомиздат, М., 1962, стр. 24.
14. *О.П.Лейпунский, Л.Р.Кимель, А.М.Панченко*, журнал "Атомная энергия", 14, (1963), 577.
15. *Л.Р.Кимель, А.М.Панченко, В.П.Терентьев*, журнал "Атомная энергия", 15 (1963), 328.
16. *А.П.Суворов, Е.Б.Бреженкова, В.В.Орлов*, статья в сб. "Вопросы физики защиты реакторов" под ред. *Д.Л.Бродера* и др., Госатомиздат, М., 1963, стр. 30.
17. *В.П.Машкович, В.К.Сахаров, С.Г.Цыпин*, статья в сборнике "Вопросы физики защиты реакторов", под ред. *Д.Л.Бродера* и др. Госатомиздат, М., 1963, стр. 182.
18. *Л.Р.Кимель, О.П.Лейпунский*, статья в сборнике "Вопросы физики защиты реакторов", под ред. *Д.Л.Бродера* и др., Госатомиздат, М., 1963, стр. 220.
19. *С.Г.Цыпин*, статья в сборнике "Вопросы физики защиты реакторов", под ред. *Д.Л.Бродера* и др., Госатомиздат, М., 1963, стр. 243.
20. *Л.Р.Кимель, А.М.Панченко, В.П.Терентьев*, статья в сб. "Вопросы дозиметрии и защиты от излучений", под ред. *В.И.Иванова*, вып. 2, Госатомиздат. М., 1963, стр. 6 и 26.
21. *И.Г.Дядькин*, ЖЭТФ, 34 (1958), 1504.
22. *В.В.Орлов, Г.И.Марчук*, статья в сборнике "Нейтронная физика", под ред. *П.А.Крупчицкого*, Госатомиздат, М., 1961, стр. 30.
23. *А.М.Панченко*, журнал "Атомная энергия", 14, (1963), 408.
24. *А.П.Лейпунский, В.Г.Грабин* и др. Экспериментальные быстрые реакторы в СССР. В кн.: Тр. Второй Международной конференции по мирному использованию атомной энергии. Доклады советских ученых т.2. Ядерные реакторы и ядерная энергетика. М., Атомиздат (1959), 215.
25. *Гольдштейн*. Основы защиты реакторов. М., Госатомиздат, (1961).
26. *Б.И.Синицын, С.Г.Цыпин*, "Атомная энергия", 12, (1962), 306.
27. *Л.П.Абагян, Н.О.Базазянц, И.И.Бондаренко, М.Н.Николаев*, Групповые константы для расчета ядерных реакторов, М., Госатомиздат, (1964).
28. *П.В.Горбсев, Д.А.Кардашев, А.В.Малышев*, Справочник по ядернофизическим константам для расчетов реакторов, М., Атомиздат, (1960).
29. *В.А.Дулин, Ю.А.Казанский* и др. П.Т.Э. №2 (1961), 35.
30. *В.А.Дулин, Ю.А.Казанский, И.В.Шугар*, "Атомная энергия", 14, (1963), 488.
31. *А.Т.Баков, С.П.Белов* и др. "Атомная энергия", 13 (1962), 31.
32. *А.А.Абагян, В.В.Орлов, Г.Н.Родионов*. О функциях опасности нейтронов при расчете защиты от излучений, в сб. статей "Вопросы физики защиты реакторов". М., Госатомиздат, (1963), 7.
33. *R.E.Lynch* et. al. A Monte Carlo Calculation of Air-Scattered Gamma, Rays. ORNL, I (1958).
34. *C.D.Zerby*. A Monte Carlo Calculation of Air-Scattered Neutrons, ORNL-2277 (1957).
35. *F.L.Keller, C.D.Zerby* and Hilgenman J. Monte Carlo Calculation of Flux and Dose Rates Resulting from Neutrons Multiple Scattered in Air, ORNL-2375 (1958).
36. *C.R.Mehl*. A Monte Carlo Calculation of the Neutron Flux from a Monoenergetic Point Source in Air, SC-4174 (TR), (1958).
37. Nucleonics, (1962), 20, 158.

38. *Л.Л.Бродер, С.А.Куркин* и др. Изучение пространственно-энергетических распределений нейтронов в различных средах. В кн.: "Тр. Второй Международной конференции по мирному использованию атомной энергии". Доклады советских ученых т.2–Ядерные реакторы и ядерная энергетика М., Атомиздат, (1959), 67.
39. *М.И.Шальнов*, Тканевая доза нейтронов, Госатомиздат, М., 1960.
40. *А.И.Веселкин, В.А.Егоров, Ю.В.Орлов, В.В.Панкратьев*, "Атомная энергия", 16, (1964), 32.
41. *В.И.Аваев, Г.А.Васильев, А.И.Веселкин, В.А.Егоров, В.В.Орлов, В.В.Панкратьев*. "Атомная энергия", 15, (1963), 20.
42. *Х.Д.Андросенко, Г.И.Смиренкин*, "Приборы и техника эксперимента", №5, (1962), 64.

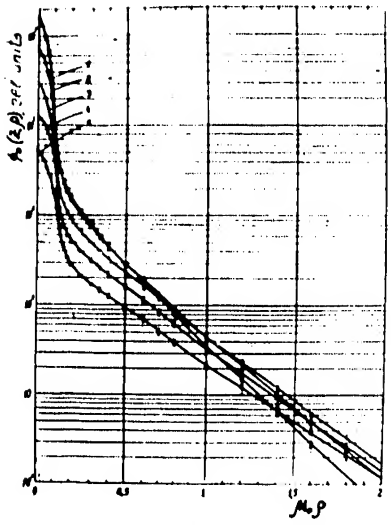

Fig.1.Narrow ray distribution function in aluminium for initial gamma-quantum energy 2,76 Mev for the distance μZ(in the mean free path length): 1 - 0,88; 2 - 1,37;3 - 2,35;4 - 2,77;5 - 3,4.

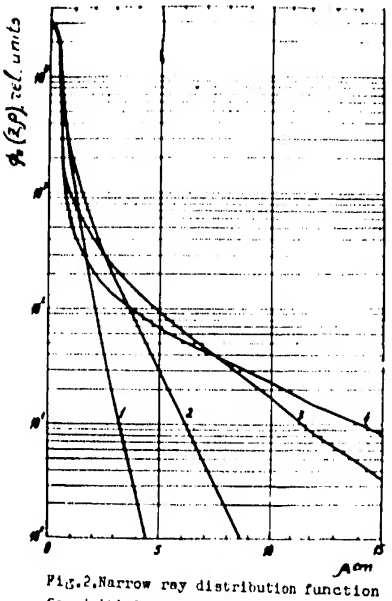

Fig.2.Narrow ray distribution function for initial gamma-quantum energy 1,25Mev due to ρ for $\mu Z=2$ for materials 1-lead, 2-iron,3-aluminium,4-water.

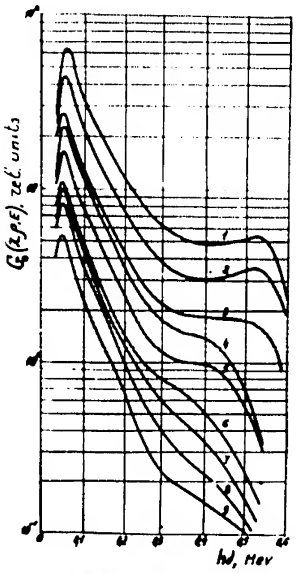

Fig.3.Space energy distribution function of narrow ray in water for gamma-quantum with initial energy 0,66 Mev for points with co-ordinates in cm:
1-Z=19,1, ρ=10,0;2-Z=29,1, ρ=10,0;
3-Z=39,1, ρ=10,0;4-Z=19,1, ρ=20,0;
5-Z=29,1, ρ=20,0;6-Z=39,1, ρ=20,0;
7-Z=19,1, ρ=30,0;8-Z=29,1, ρ=30,0;
9-Z=39,1, ρ=30,0.

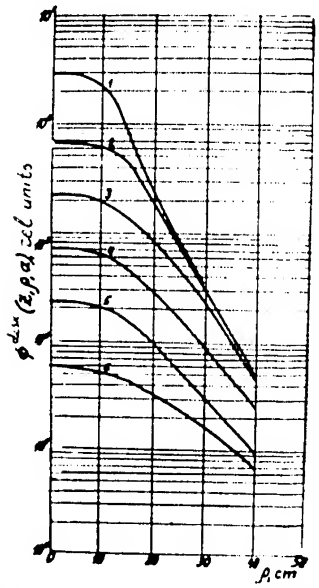

Fig.4.Distribution function of disc monodirectional neutron fission source in water according to the indicator measurements by the reaction $P^{31}(n,p)Si^{31}$ for Z in cm: 1 - 16,5;2 - 30,0; 3 - 40,0;4 - 50,0; 5 - 60,0;6 - 72,5.

377

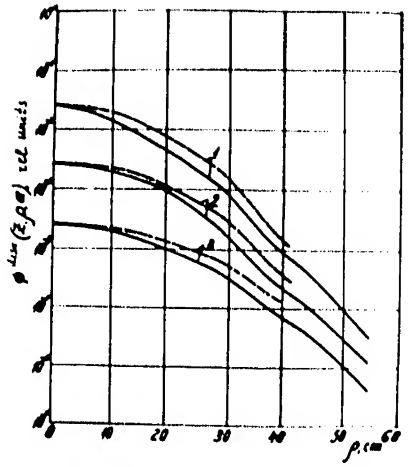

Fig.5.Calculated and experimental data comparison (solid curves -calculation by the momentum method;dotted curves - experimental data)according to the indicator data by the reaction $Al^{27}(n,\alpha)Na^{24}$ in different planes Z depending on the distance to the central beam ρ for line monodirectional source for Z in cm: 1 - 27,1 cm;2 - 34,6 cm; 3 - 50,5 cm.

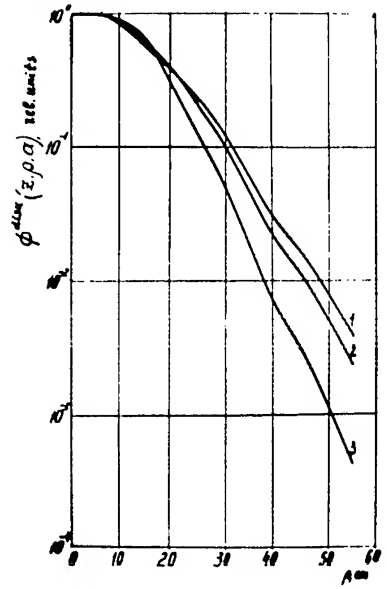

Fig.7.Distribution function of disc mondirectional neutron fission source according to the indicator measurements by the reaction $S^{32}(n,p)P^{32}$ depending on ρ for Z=30 cm for materials: 1 -carbon;2 - iron;3 - water.

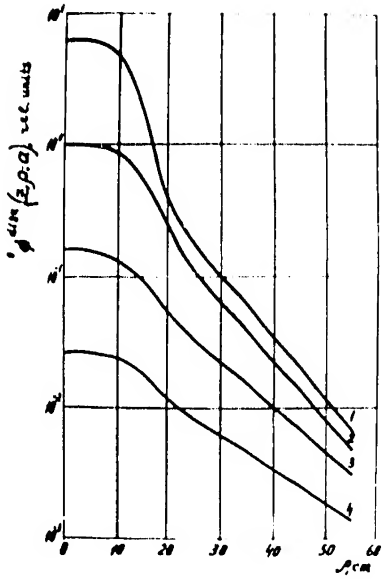

Fig.6.Distribution function of disc monodirectional neutron fission in carbon according to the indicator measurements by the reaction $S^{32}(n,p)P^{32}$ for Z in cm: 1 - 10,0; 2 - 30,0; 3 - 50,0; 4 - 70,0.

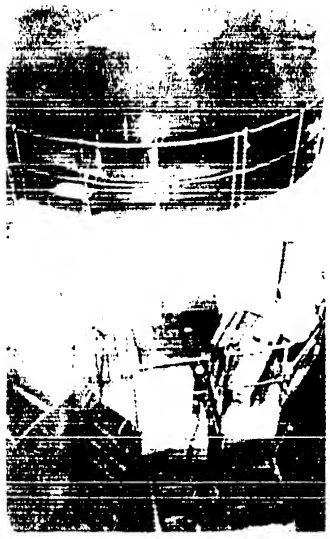

Fig.8.The facility Б-2 for Shielding investigations.

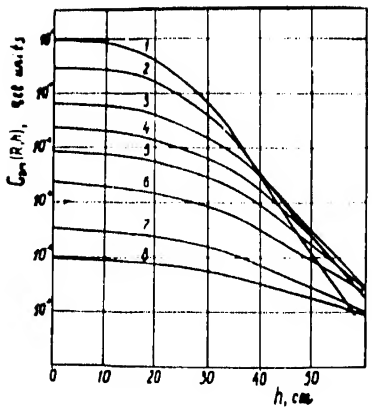

Fig.9.Attenuation function of the mono-directional fission spectrum source for different thicknesses of lithium hydride R measured by the threshold detector $P^{31}(n,p)Si^{31}$ (h - the distance from the disc axis). 1.R=16,5cm;2.R=26,5 cm.3.R=39,5cm. 4.R=49,5cm.5.R=59,5cm. 6.R=72cm. 7.R=82,5cm.8.R=92,5cm.

Fig.10.General view of the reactor "PU3"

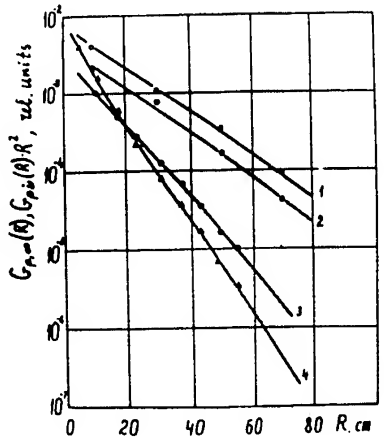

Fig.11.Fast neutron flux distributions in lithium hydride (ρ =0,82 g/cm^3) and in carton (ρ =1,67 g/cm^3) from neutron fission source.

Lithium Hydride

3 - the detector measurements $Al^{27}(n,d)Na^{24}$. The source is plane,monodirectional

4 - dose calculation by the momentum method[9] from the point isotropic source. The geometry was eliminated by the multiplication by R^2.

▲- The detector measurements $P^{31}(n,p)Si^{31}$ Si^{31} and $S^{32}(n,p)P^{32}$.The source is plane,mondirectional.

Carbon.

1.Calculation by the momentum method [25] for the reaction $S^{32}(n,p)P^{32}$.The geometry was eliminated by the multiplication on R^2.

○-the indicator measurements $S^{32}(n,p)P^{32}$. The source is plane,monodirectional

2.Calculation by the momentum method [25]for the reaction $Al^{27}(n,d)Na^{24}$.

The geometry was eliminated by the multiplication on R^2

● the indicator measurements $Al^{27}(n,d)Na^{24}$ The source is plane,monodirectional.

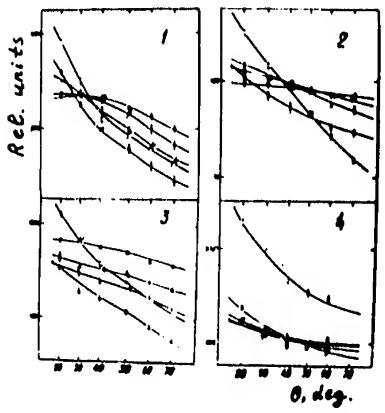

Fig.12,The angular distribution of energetic neutron groups for water(1), carbon(2),iron(3) and lead (4). o - group 3,1-3,4Mev;e-2,1-3,1Mev; ▲ - 1,4-2,1 Mev;e -0,8-1,4Mev; ■ - 0,5-0,8Mev.

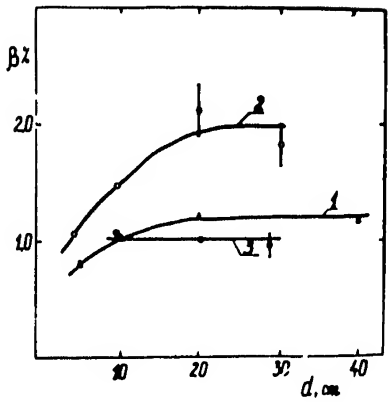

Fig.13.Secondary rediation factor dependence from the shield thickness of iron (1),nickel (2) and nickel with 2%,boron by weight (3).

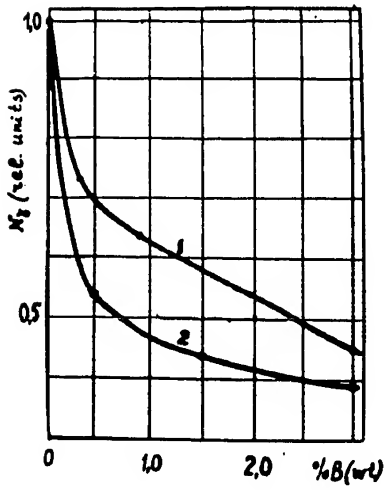

Fig.14.Capture gamma radiation relative yield from iron (1) and nickel (2) depending on boron weight content.

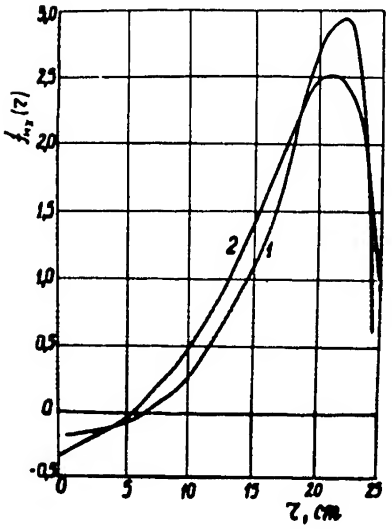

Fig.15.Experimental (1) and calculated (2) functions of hydrogen efficiency (0,11 g/cm^2) in nickel.

377

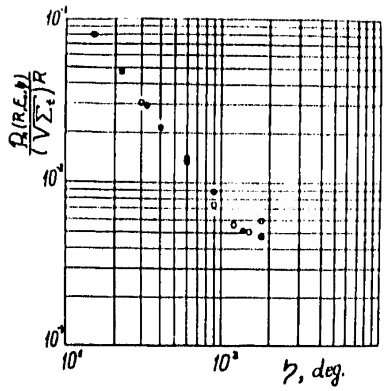

Fig.16. Relative dose rate space distribution of neutrons scattered in the air for monodirectional source. O - the authors' experimental data, E_0=14,2 Mev o - calculated data (*) averaged out of initial energy intervals from 0,35 to 6 Mev.

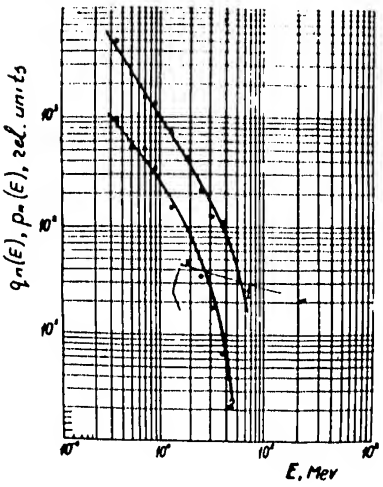

Fig.17. Energetic distribution of neutrons scattered in the air from the point isotropic source. Monodirectional detector.
E_0=1,3Mev, R=14,3 m o - ψ =30°
● - ψ =180°.
The authors' experimental data.
Energetic distribution of neutrons scattered in the air from the monodirectional source. According to the calculated data [9] E_0=1,3Mev R=14,3m. Curve 1 ϑ = 30°, Curve 2 - ϑ = = 180°.

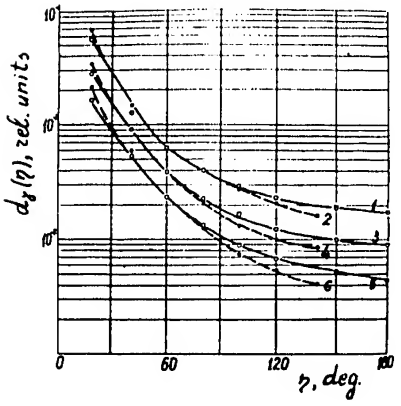

Fig.18. Dose rate space distribution of gamma radiation scattered in the air from the monodirectional source.

1-R=0,1 λ ,	E_0=0,411 Mev*/	2-R=1 λ ,	E_0=0,411 Mev	[10]
3-R=0,1 λ ,	E_0=1,25Mev*/	4-R=1 λ ,	E_0=1,25Mev	[10]
5-R=0,1 λ ,	E_0=1,9Mev*/	6-R=0,8 λ ,	E_0=1,9Mev	[10]

*/ the Author's data.

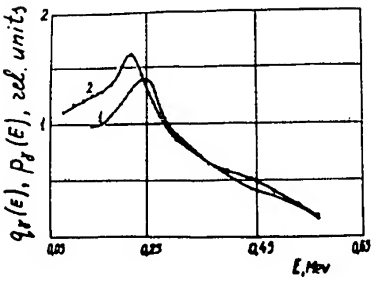

Fig.19. Energetic distribution of gamma rays scattered in the air from the monodirectional source. Isotropic detector.
R = 16m, ϑ =60° E_0=1,25Mev - curve 1.
Energetic distribution of gamma rays scattered in the air from the isotropic source (monodirectional detector) for R=16m, x=60°, E_0=1,25Mev, curve 2 the Authors' data.

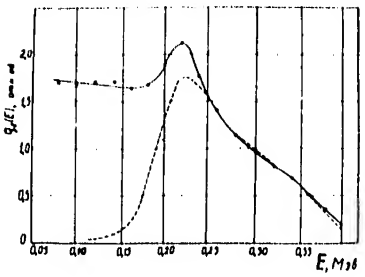

Fig.20.Energetic distribution of gamma rays scattered in the air from the isotropic source (monodirectional detector) for E_0=1,2 Mev. o – experimental data, —— the calculation in the single approximation. Calculated discription is normalized to the experimental one at E=0,3 Mev. the Authors' data.

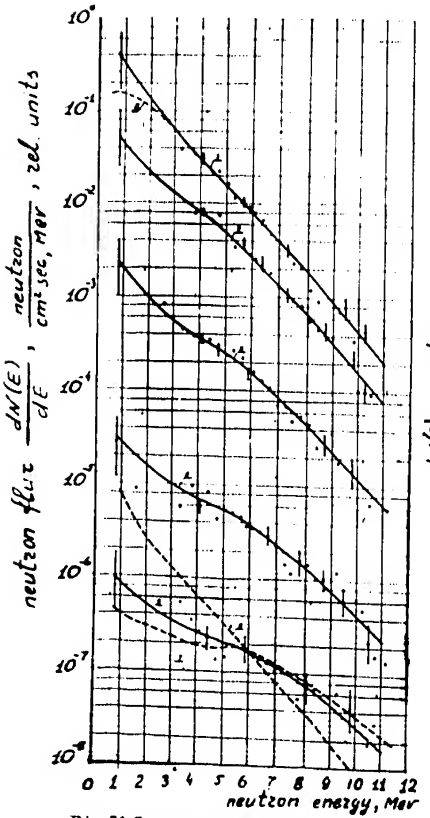

Fig.21.Fast neutron energetic distribution in the mixture polyethylene + iron.
● – neutron fission spectrum.
1 – thickness 0 g/cm², 2.–24,9 g/cm², 3–81 g/cm², 4 – 147 g/cm², 5 – 2[illegible] g/cm², 6 – the spectrum after the iron layer 243 g/cm², 7 – the spectrum after the polyethylene layer 72 g/cm².

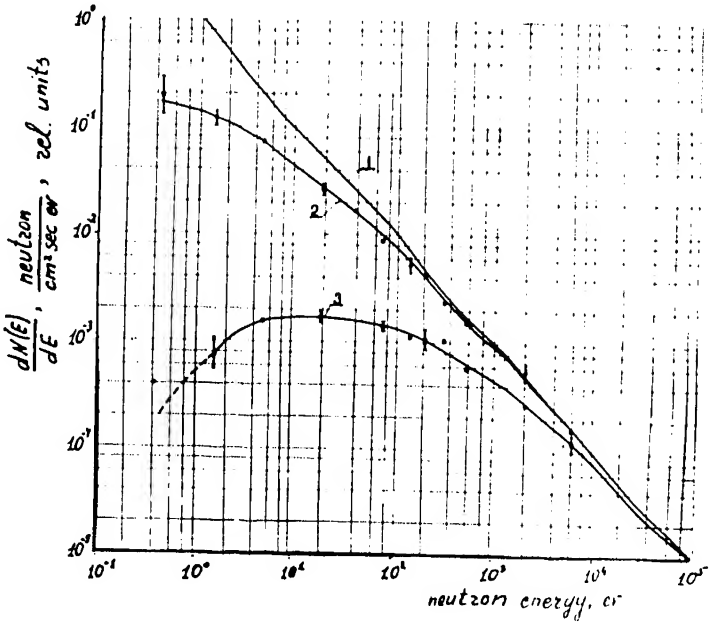

Fig.22.Epithermal neutron distribution in iron (2), in graphite with boron (3) and the spectrum 1/E (1).